Thesis for Master Degree

Phase Equilibrium, Spectroscopic Investigation, and Formation Kinetics of $CHClF_2$ Hydrate in Chloride Ion Solution

염소이온용액에서 형성된 클로로디플루오로메탄 하이드레이트의 상평형, 분광학적 분석 및 형성역학에 관한 연구

Advisor: Prof. Yoon, Ji-Ho

February 2019

Department of Convergence Study on the Ocean Science and Technology
School of Ocean Science and Technology
Korea Maritime and Ocean University

Woo, Yesol

Thesis for Master Degree

Phase Equilibrium, Spectroscopic Investigation, and Formation Kinetics of $CHClF_2$ Hydrate in Chloride Ion Solution

염소이온용액에서 형성된 클로로디플루오로메탄 하이드레이트의 상평형, 분광학적 분석 및 형성역학에 관한 연구

Advisor: Prof. Yoon, Ji-Ho

February 2019

Department of Convergence Study on the Ocean Science and Technology
School of Ocean Science and Technology
Korea Maritime and Ocean University

Woo, Yesol

Approved by the Committee of the Ocean Science and Technology School of Korea Maritime and Ocean University in Fulfillment of the Requirements for the Degree of Master´ s in Engineering

Dissertation Committee :

Prof. Yoo, Kyoungkeun, Chair _____

Prof. Yoon, Ji-Ho, Advisor _____

Prof. Kim, Dongseon, Advisor _____

February 2019

Department of Convergence Study on the Ocean Science and Technology

Ocean Science and Technology School

Korea Maritime and Ocean University

Table of Contents

List of Tables

List of Figures

염소이온용액에서 형성된 클로로디플루오로메탄 하이드레이트의 상평형, 분광학적 분석 및 형성역학에 관한 연구

우 예 솔

해양과학기술융합학과
한국해양대학교 해양과학기술전문대학원

초 록

본 연구에서는 가스하이드레이트 기반의 담수화 공정을 위한 연구를 수행하였다. 하이드레이트의 게스트 분자로는 하이드레이트 형성 조건을 현저히 완화시키는 클로로디플루오로메탄(Chlorodifluoromethane, $CHClF_2$, R22)을 이용하였으며 해수 조성의 대부분을 차지하는 염화나트륨, 염화마그네슘, 그리고 니켈 전기도금의 폐수로서 방출되는 염화니켈을 목표 염분으로 하여 연구를 진행하였다. 하이드레이트 담수화 공정에 필수적으로 요구되는 하이드레이트의 열역학적 안정영역을 파악하기 위해 염화니켈 수용액의 각 농도별 (0, 5, 10, 그리고 15 wt%) 환경에서 형성된 R22 하이드레이트 3상 (H-Lw-V)의 상평형 점을 측정하였으며 R22 하이드레이트의 구조에 염분이 영향을 미치지 않음을 증명하기 위해 X-ray diffraction (XRD)과 Raman spectroscopy로 염화나트륨, 염화마그네슘, 그리고 염화니켈 각 0, 5, 그리고 10 wt% 수용액 환경에서 형성된 R22 하이드레이트 시료를 분석하였다. 그 결과 염분을 첨가하지 않은 R22 하이

드레이트의 결과와 비교했을 때 어떠한 구조적인 변화도 관찰되지 않음을 확인했다. 또한 각 농도별 염분 수용액에서 형성된 R22 하이드레이트의 형성속도를 알아내고, 또 예측하기 위해 새로운 속도 모델을 제시하였으며 실제 하이드레이트 형성 실험결과와 모델을 통해 계산된 결과를 비교하였다. 그 결과 속도 모델이 실제 하이드레이트 형성 예측에 잘 적용됨을 확인 하였다. 본 연구를 통해 얻은 염화니켈 수용액 환경에서 형성된 R22 하이드레이트의 상평형 지점 및 형성 속도 예측에 관한 모델, 그리고 모델을 통해 얻은 구체적인 수치는 추후 유사한 하이드레이트 기반의 분리 공정에 기초 데이터로 활용될 수 있을 것으로 사료된다.

Key Words : Chlorodifluoromethane 클로로디플루오로메탄, Clathrate hydrate 포접 수화물, Hydrate-based desalination 하이드레이트 기반의 담수화, Phase equilibrium 상평형, Spectroscopic identification 분광학적 분석, Formation kinetic 형성 역학.

Chapter 1. Introduction

1.1 Background

1.1.1 Clathrate Hydrate

Clathrates, which are crystalline inclusion compounds stabilized by interactions between host and guest molecules in the host framework architecture, have been studied as practically beneficial and environmentally sustainable media for gas storage over the past few decades (Atwood, et al., 1984; Berecz & Bella-Achs, 1983; Sloan, 2003). Clathrate structures possess suitably sized cages that can trap relatively small molecules such as carbon dioxide, methane, and nitrogen and large hydrocarbons such as adamantine and methylcyclohexane in the hydrogen-bonded framework.

Clathrate hydrate is a solid ice-like compounds composed of hydrogen-boned water molecules (host) and gas molecules (guests) such as methane, ethane, propane, carbon dioxide, etc (Fig. 1). As shown in Fig. 2, On the basis of differences in the sizes and shapes of the hydrate cages, they are commonly classified into three main structural types: structure I (sI), structure II (sII), and structure H (sH) (Sloan, 1988; Ripmeester, et al., 1987; Berecz & Bella-Achs, 1983). Jeffrey (1984) suggested the nomenclature description (n_i^{mi}), for these polyhedra, where n_i is the number of edged in face type i and m_i is the number of faces with n_i edges. The cubic sI hydrate structure contain sixteen 5^{12} cavities, eight $5^{12}6^4$ cavities and 136 H_2O molecules per unit cell, and cubic sII hydrate structure contain sixteen 5^{12} cavities, eight $5^{12}6^4$ cavities and 136 H_2O molecules per unit cell. The hexagonal sH unit cell, has composotion of three 5^{12} cavities, two $4^3 5^6 6^3$ cavities, one $5^{12}6^8$ cavity and 34 H_2O molecules per unit cell, and

containing even larger molecules such as 2,2-dimethylbutane in the large cavities only (Sloan, 1988; Udachin, et al., 2002). The crystal properties of sI, sII, and sH are given in Table 1 detail. As shown in Fig. 3, the cavities occupancy of gas hydrate depends on the size of the guest molecules (von Stackelberg, 1949; Ripmeester, et al., 1987). The gas hydrate was first identified in 1811 by Humphrey Davy. After that, it was discovered that natural gas hydrates lead to the plugging of gas pipelines in the petroleum process (Hammerschmidt, 1934) and a self-preservation enables gas hydrates to encapsulate gases at atmospheric pressure (Davidson, et al., 1986), consequently, many researchers have become interested in studying hydrates as promising functional materials for the storage and transportation of gas in the form of gas hydrates (Ganji, et al., 2007; Javanmardi, et al., 2005).

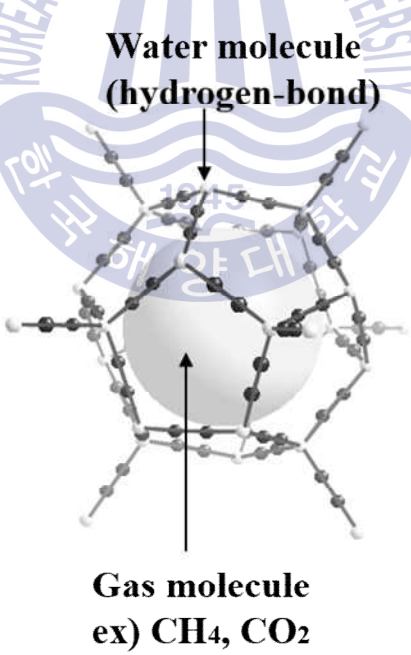

Fig. 1 Bonding diagram of clathrate hydrate

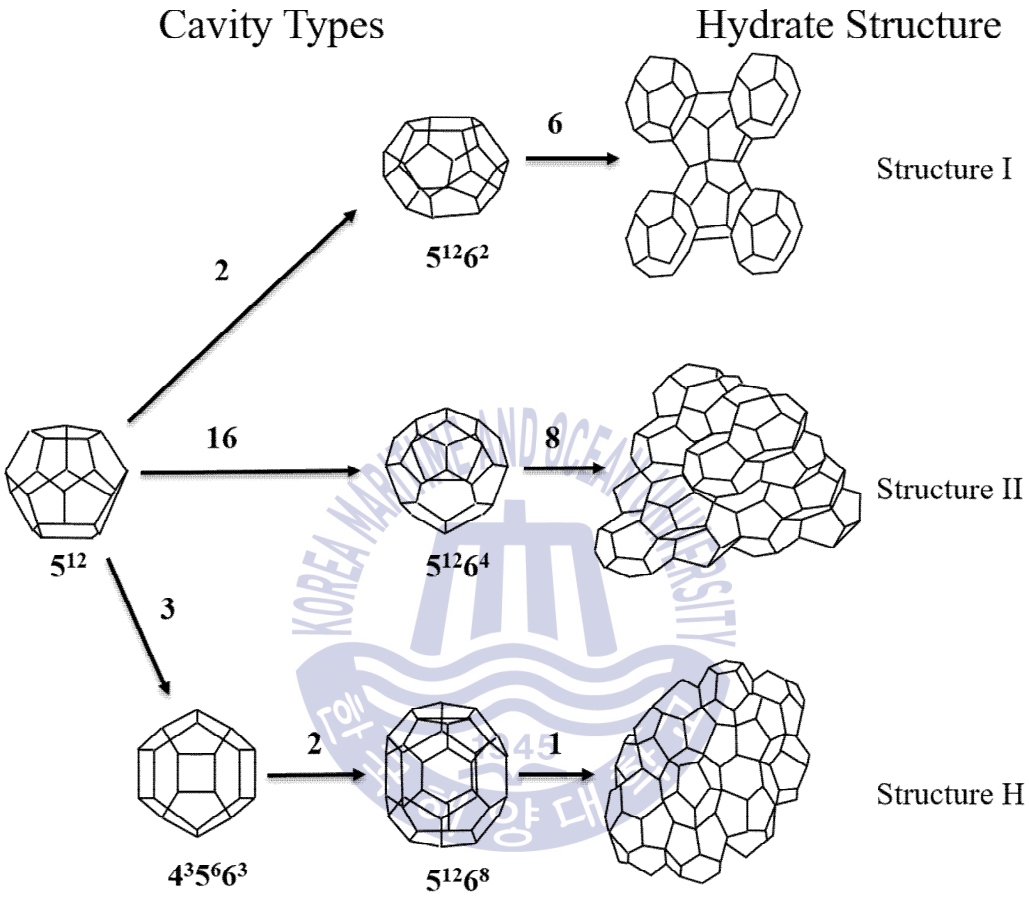

Fig. 2 Cavity types and structure of clathrate hydrate (Sloan, 1988; Ripmeester, et al., 1987; Berecz & Bella-Achs, 1983)

Table 1 Crystal properties of sI, sII, and sH (Sloan, 1988)

Hydrate Crystal Structure	**I**		**II**		**H**		
Crystal Type	Cubic		Cubic		Hexagonal		
Space Group	*Pm3n*		*Fd3m*		*P6/mmm*		
Lattice Parameters (Å)	a = 12		a = 17.3		a = 12.2, c = 10.1		
Cavity	Small	Large	Small	Large	Small	Medium	Large
Description	5^{12}	$5^{12}6^2$	5^{12}	$5^{12}6^4$	5^{12}	$4^35^66^3$	$5^{12}6^8$
Number of Cavities	2	6	16	8	3	2	1
Average Cavity Radius (Å)	3.95	4.33	3.91	4.73	3.94	4.04	5.79
Coordination Number	20	24	20	28	20	20	36
Idea gas composition	$6X \cdot 2Y \cdot 46H_2O$		$8X \cdot 16Y \cdot 136H_2O$		$1X \cdot 3Y \cdot 2Z \cdot 34H_2O$		

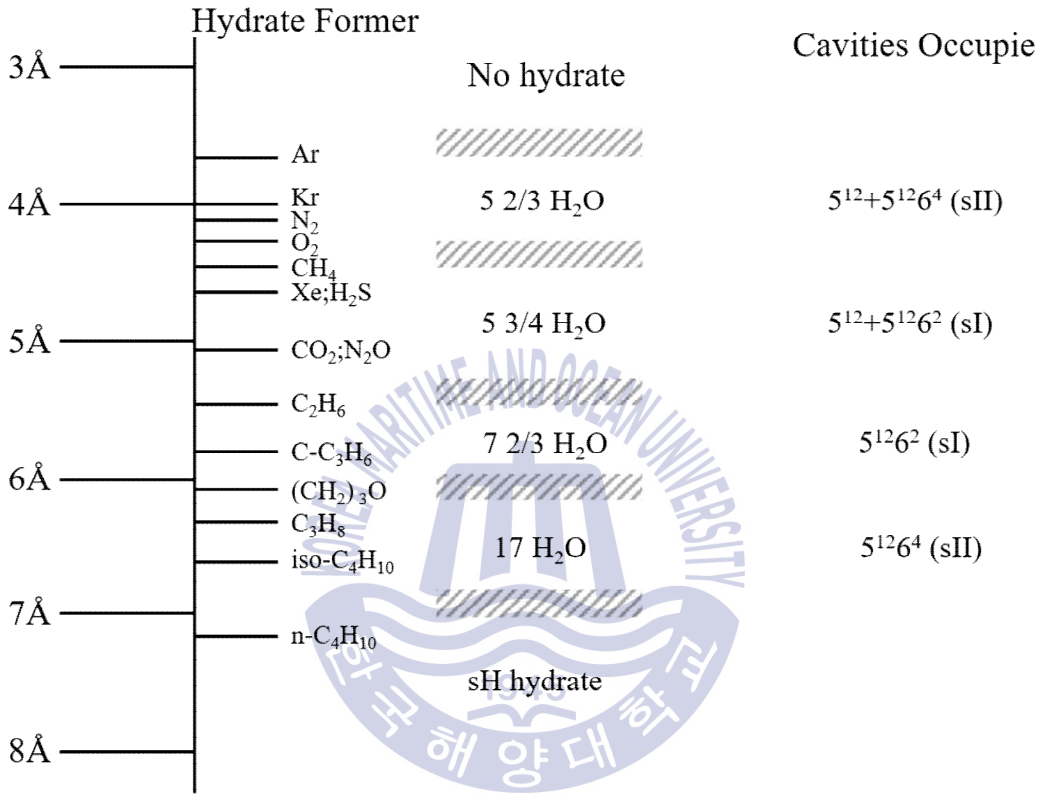

Fig. 3 Correlation between size of guest molecules and hydrate cavities occupation (Stackelberg, 1949; Ripmeester et al., 1987)

1.1.2 Desalination

Over the last several decades, due to increased population as well as the large expansion in industrial activities, the provision of fresh water is becoming an increasingly important issue in many countries of the world (Park, et al., 2011; Kalogirou, 2005; Oki & Kanae, 2006). Seawater accounts for about 97% of the overall global water and only about 0.5% of the overall global water are available as fresh water (Zhou, 2015; Kalogirou, 2005). Therefore, during the last decades, seawater has become an important source of fresh water in many arid regions (Van der Bruggen & Vandecasteele, 2002). In addition, the majority of the world desalination installation capacity is for desalting of seawater (59%), followed by brackish water (22%), with the remainder (19%) being for river water, wastewater, and potable water (VirgiliPankratz & Gasson, 2016).

The method of seawater desalination is largely classified according to the main two basic principle: thermal distillation (Multi-Stage Flash and Multi-Effect Distillation) and membrane separation (Reverse Osmosis). Also, there are hybrids plants which integrate thermal and membrane technologies (Hamed, 2005). MSF came into practice in the early 1960s and became the most common process for seawater desalination for the next few decades, due to its reliability and simplicity (Al-Wazzan & Al-Modaf, 2001). Despite the wide use of thermal technologies including MSF, membrane based technologies are becoming more popular in areas like the Middle East due to their lower specific energy consumption, lower environmental footprint, and more flexible capacity (Eveloy, et al., 2015). With these improvements in rival technologies as RO, the installation of MSF plants is on a downward trend (Mezher, et al., 2011). As shown in Fig. 4, RO has emerged as the leading desalination technology practiced today (65%),

followed by multi-stage flash evaporation (21%). The remaining 14% of the capacity include multiple effect distillation, vapor compression, and electrodialysis (ED)/ED reversal (EDR) (VirgiliPankratz & Gasson, 2016).

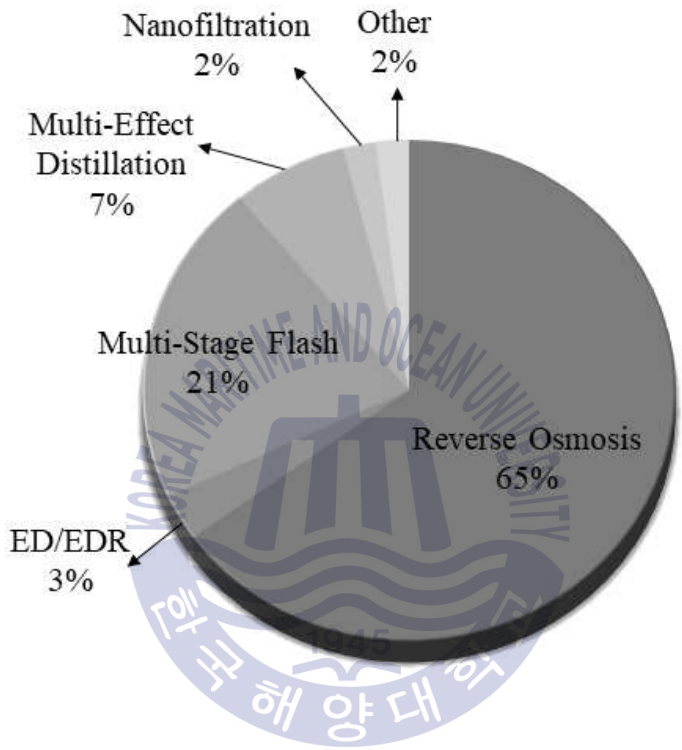

Fig. 4 Desalination capacity by technology (VirgiliPankratz & Gasson, 2016)

1.1.3 Hydrate-Based Desalination

Among the various desalination approaches, hydrate-based desalination (HBD) technology is a promising method for recovering freshwater from sea water. Fig. 5 shows the potential of HBD process based on performance in comparison with Multistage distillation (MSF), reverse osmosis (RO). HBD, the cost of producing one ton of potable water is comparable to the more mature RO and is significantly lower than MSF (Babu, et al., 2018). In addition to seawater desalination, the HBD technology can be applied to separating heavy metals from aqueous solutions, especially in the treatment of electroplating wastewater (Song, et al., 2016). Nickel electroplating effluent contains large amounts of nickel chloride (Ahn, et al., 1999; Benvenuti, et al., 2014), which are non-biodegradable and bio-accumulative. HBD technology is regarded as an environmental-friendly method because hydrates can be directly formed from seawater under low-temperature and high-pressure conditions (Seo, et al., 2015; Park, et al., 2011) and it is based on the simple principle that only water and gas molecules participate in the formation of the hydrate crystal structure (Fig. 6). Although the HBD technology is at the developmental stage compared to well-established commercially available techniques, it still draws attention because of its simplicity, eco-friendliness and economics, especially when using refrigerants for guest molecules.

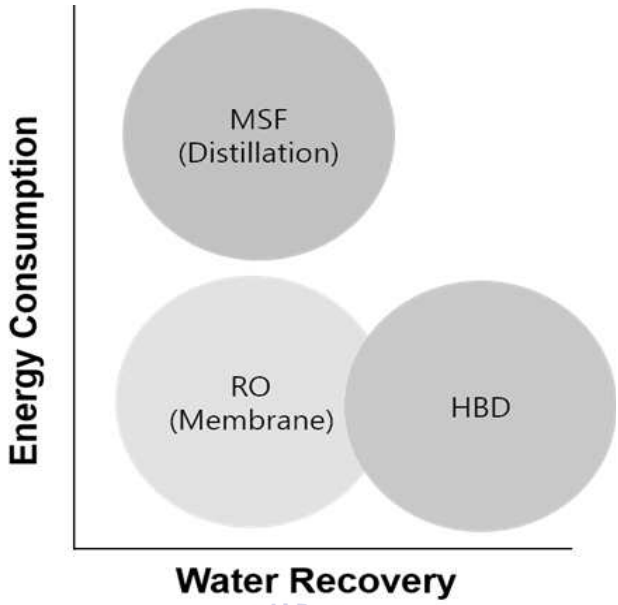

Fig. 5 Potential of HBD process based on performance in comparison with MSF and RO (Babu, et al., 2018)

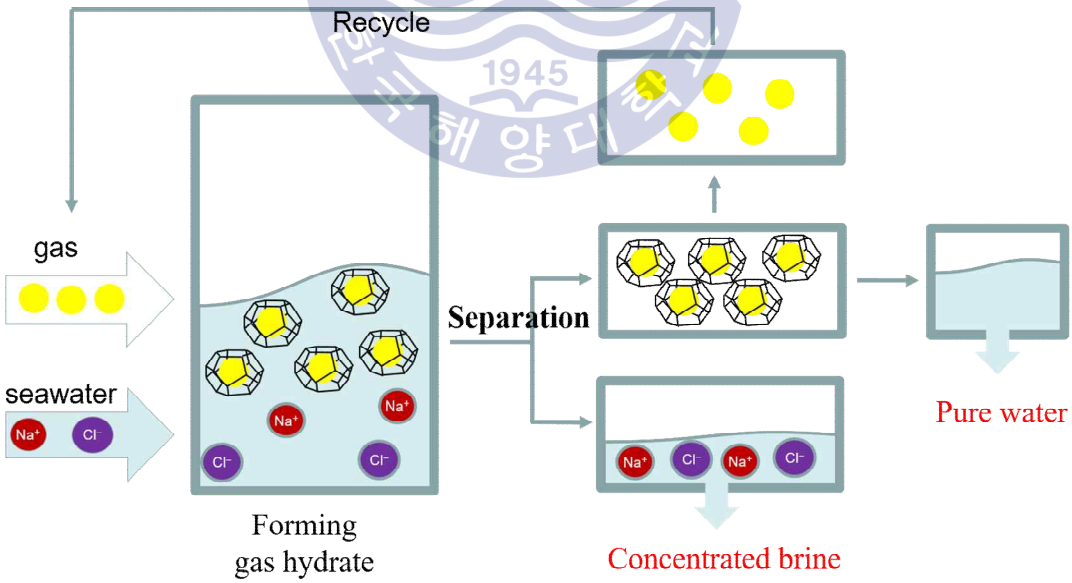

Fig. 6 Principle of hydrate-based desalination

1.1.4 $CHClF_2$

Chlorodifluoromethane ($CHClF_2$) is well-known gas due to its contribution to ozone depletion and global warming (Merke, et al., 1995; Snels & D'Amico, 2001; UNEP, 2000). $CHClF_2$ form the sI hydrate, and can be only captured in the large cages of sI the hydrate due to the larger size than the small cages of the sI hydrate (Wittstruck, et al., 1961). Achieving the appropriate high-pressure condition for gas hydrate formation is a major obstacle to improving hydrate formation efficiency; therefore, the development of an efficient way to form gas hydrates under more moderate conditions is one of the key objectives of the HBD technology. In this sense, generally, refrigerants including $CHClF_2$, trichlorofluoromethane (CCl_3F) and dichlorodifluoromethane (CCl_2F_2), can be considered as potential hydrate formers for HBD process, because most refrigerant hydrates can be stable under relatively mild conditions (Merke, et al., 1995; Eslamimanesh, et al., 2011; Karamoddin & Varaminian, 2014). Therefore, the use of $CHClF_2$ for HBD process could lead to the dual benefits of greenhouse gas control and hydrate-based desalination. Fig. 7 shows the phase equilibrium conditions of $CHClF_2$ (R22) hydrates are milder than those of conventional gas hydrates, such as methane, carbon diaxide, nitrogen hydrates. Therefore, the use of $CHClF_2$ can reduce the energy required for the HBD process.

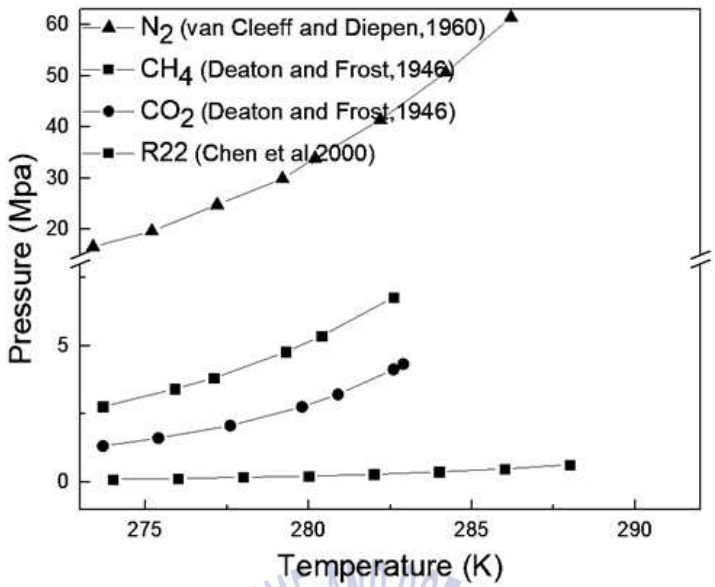

Fig. 7 Phase equilibria of many gas hydrate

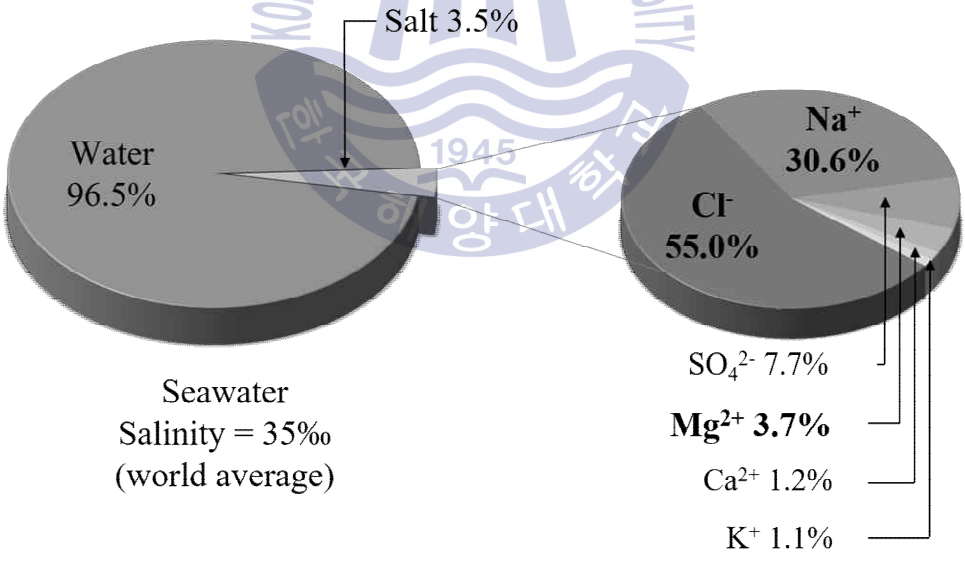

Fig. 8 Chemical composition of seawater (weight ratio)
(Andrea, et al., 2005)

1.2 Purpose

As shown in Fig. 8, the most abundant dissolved ions in the seawater are sodium, chloride, magnesium and sulfate. Thus, for desalination of seawater and nickel electroplating effluent, I decided to do research about hydrate formed in NaCl, $MgCl_2$, and $NiCl_2$ brine solutions. In the procedure of hydrate-based desalination, the formed gas hydrate needs to be regasified after hydrate formation, and fresh water is recovered through hydrate dissociation (Seo, et al., 2015). Therefore, complete understanding the hydrate formation kinetics and the hydrate formation/dissociation boundaries are very important. There are no researches on the phase equilibria of the $CHClF_2$ hydrate in the presence of $NiCl_2$, whereas research on the NaCl and $MgCl_2$ have been performed. Therefore, I investigated the phase equilibrium conditions of the $CHClF_2$ hydrates formed in $NiCl_2$ brine solutions to determine the effect of $NiCl_2$ on the thermodynamic stability of the $CHClF_2$ clathrate hydrates. To apply the hydrate-based desalination process, the exclusion of the purposed salt ions from the hydrate structure should be demonstrated. The structural identification and guest partitioning of the $CHClF_2$ clathrate hydrates formed in NaCl, $MgCl_2$, and $NiCl_2$ brine solutions confirmed by X-ray diffraction (XRD) and Raman spectroscopy. I also explored the formation kinetics of the $CHClF_2$ hydrates formed in NaCl, $MgCl_2$, and $NiCl_2$ brine solutions (0, 5, and 10 wt%) to develop the HBD technology using the $CHClF_2$ hydrate.

Chapter 2. Experimental Section

2.1 Materials and Apparatus

$CHClF_2$ gas with a minimum purity of 99.8 mol % was provided by Korea Standard Gas Co. (South Korea). NaCl with a minimum purity of 99.5 mol % and $MgCl_2$ and $NiCl_2$ with a minimum purity of 98 mol % were supplied from Sigma-Aldrich. These materials were used without further purification.

Samples for analyzing Raman spectra and XRD patterns of the $CHClF_2$ hydrate were prepared with the following procedures. The high-pressure reactor cell was charged with 80-100 ml of aqueous salt solution (0, 5, and 10 wt%, respectively) and immersed in a water bath at 275 K. After completion of the cell condition stabilization, the cell was repeatedly pressurized and maintained at 5 bar with $CHClF_2$ gas during hydrate formation. When there was no change in the pressure of the cell, the cell was immersed in the liquid nitrogen to freeze the samples; then, the hydrate samples were ground into powders 100 μm or less-sized under the liquid nitrogen environment.

2.2 Experiment Method

2.2.1 Phase Equilibrium Conditions

To investigate the phase equilibrium conditions of the $CHClF_2$ hydrate formed from $NiCl_2$ aqueous solution, a high-pressure equilibrium cell with two reinforced sight glasses on both sides of the cell was used. Firstly, the cell was charged with 80 ml of $NiCl_2$ aqueous solution (0, 5, 10 and 15 wt%) and placed in the water bath held at the desired temperature. Then, the $CHClF_2$ gas was slowly injected to the desired pressure. The hydrate formation began by stirring the cell contents at the temperature far below the expected hydrate equilibrium temperature. After completion of the hydrate formation, the $CHClF_2$ hydrate was slowly dissociated by increasing the cell temperature with a rate of 0.1 K/h. Finally, when only minute hydrate particles existed in the cell and drastic change was observed in recorded Pressure-time slopes data, I decided that point is the three phase (Hydrate–Liquid water–Vapor) equilibrium conditions of the $CHClF_2$ hydrates (Fig. 9).

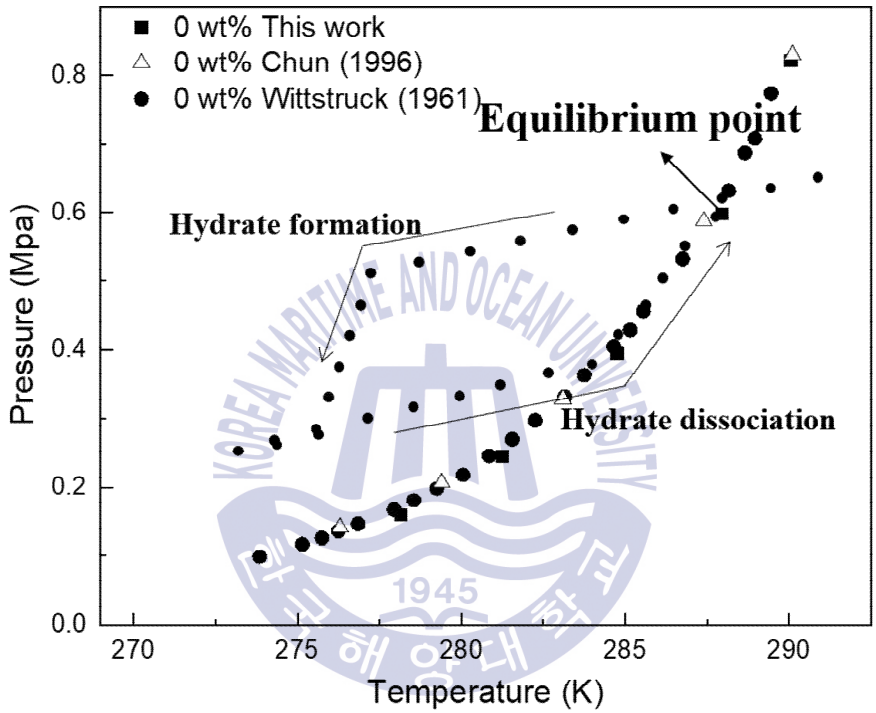

Fig. 9 Phase equilibrium point of the $CHClF_2$ hydrate

2.2.2 X-ray Diffraction

The crystal structure of the $CHClF_2$ hydrate formed in aqueous solution was identified by a high-resolution synchrotron XRD at beamline 9B of the Pohang Accelerator Laboratory (PAL). The XRD measurement can be used to reveal the atomic and molecular structure of crystals using the diffraction of incident beam of X-ray into the crystal (Fig. 10). The XRD patterns were collected in the range of 5-125.5° with a step size of 0.01° at 90 K and a wavelength of 1.5183 Å .

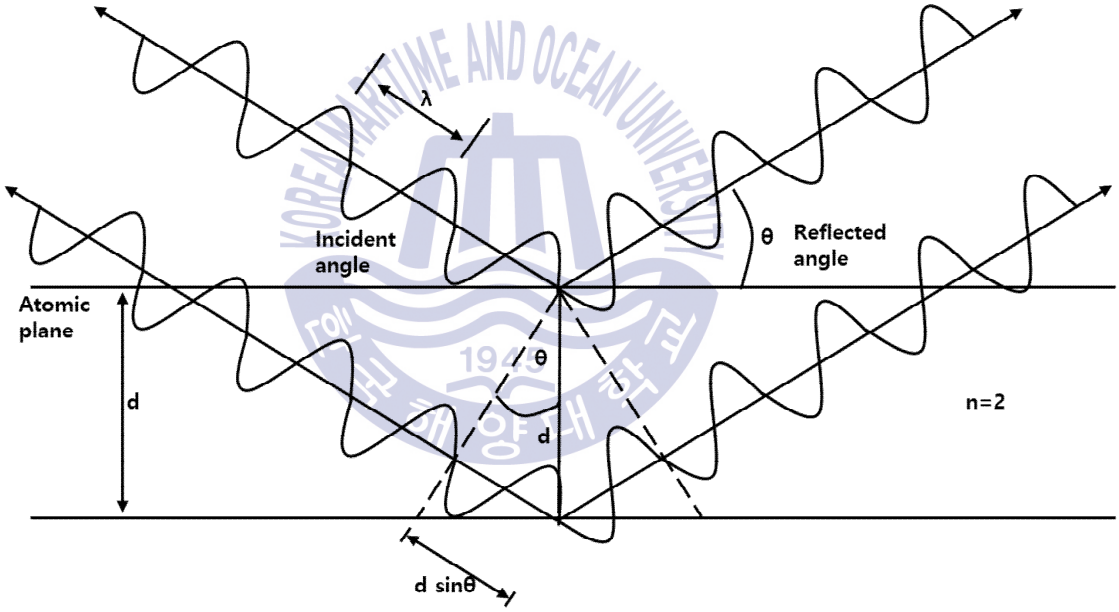

Fig. 10 Principle of X-ray diffraction

2.2.3 Raman Spectroscopy

Raman spectroscopy is one of the vibrational spectroscopic method used to provide a structural fingerprint by which molecules can be identified. When light of a single frequency is focused onto a material, the frequency of some of light that is scattered from the material may be shifted, and these frequency shifts are equal to the frequency of the inherent molecular vibrations in the sample (Yu & Krimm, 1977). As shown in Fig. 11, a customized Raman spectroscopy equipped with a multichannel air-cooled charge-couple device (CCD) detector (Princeton Instruments, PIXIS:100B) and a Nd-YAG laser emitting a 532 nm line with a maximum power of 71.6 mW was used to in this study. Using a temperature-controlled microscope stage (Linkam, THMS 600), all Raman measurements were performed at ambient pressure and 83 K.

Fig. 11 Customized Raman spectroscopy

2.2.4 Formation Kinetics

For formation kinetics of $CHClF_2$ hydrate experiment, a high-pressure reactor cell with an interval volume of 277 cm^3 was used. The cell was charged with 100 cm^3 of aqueous NaCl, $MgCl_2$, and $NiCl_2$ solution (0, 5, and 10 wt%), respectively. Then, the temperature and pressure of the cell was adjusted to 278 K and 5.2 bar, and they were kept constant for 1 h. After completion of the stabilization, the formation of the hydrates started by stirring the cell contents at a rate of 400 rpm, and the time dependent pressure drop was measured every 5 s in a real time.

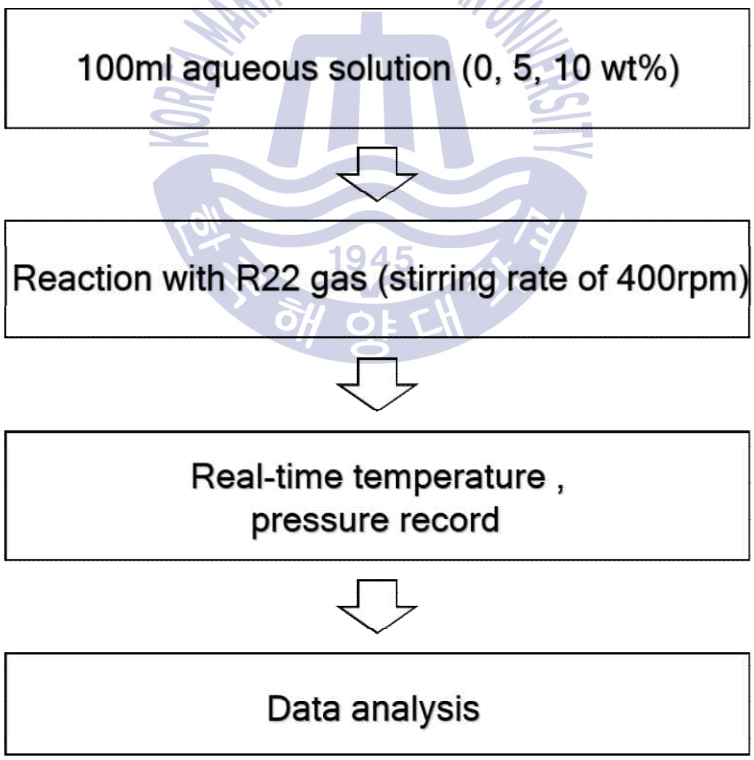

Fig. 12 Experimental procedure of formation kinetics

Chapter 3. Results and Discussion

3.1 Phase Equilibrium

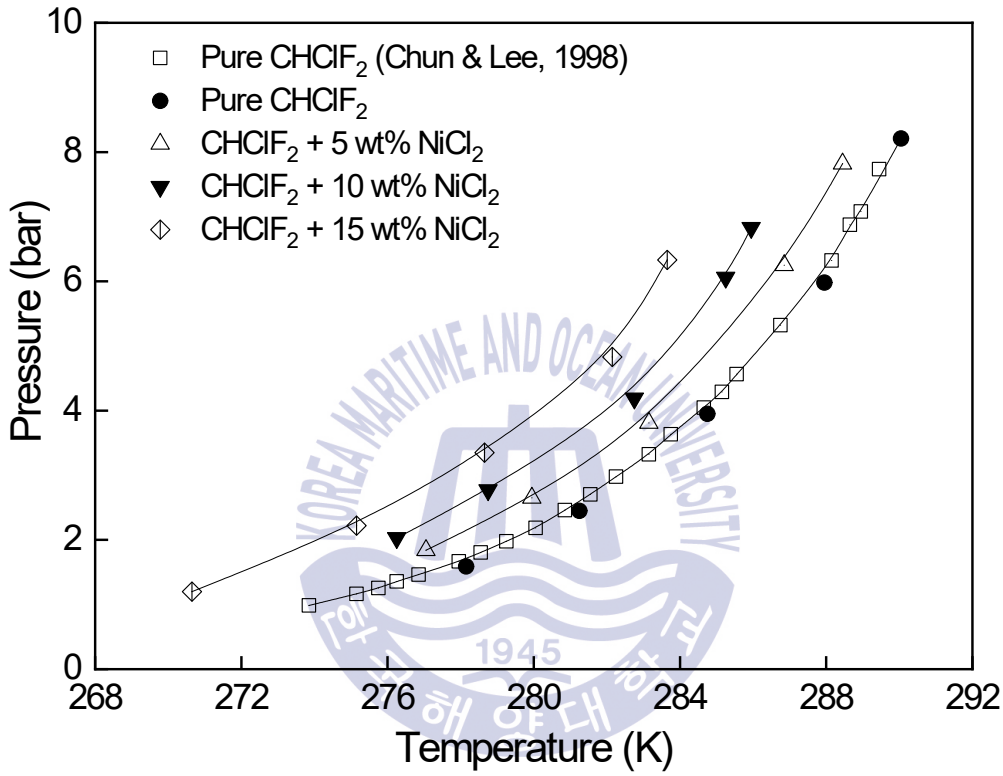

Fig. 13 Equilibrium dissociation pressures of $CHClF_2$ hydrates in the presence of $NiCl_2$ as a function of temperature. The solid lines are guide for the eyes

Fig. 13 shows the three phase (hydrate-aqueous liquid-vapor) equilibria of the $CHClF_2$ hydrate in the presence of $NiCl_2$. To confirm the validity of apparatus and experimental procedure, experimental results of pure $CHClF_2$ hydrate were compared with previous results (Wittstruck, et al., 1961), and

the results were in a good agreement. As a results, the phase equilibria of the $CHClF_2$ hydrate in the presence of $NiCl_2$ (0, 5, 10 and 15 wt%) in the temperature range of 270-293 K and the pressure range up to 8.2 bar are listed in Table 2. The hydrate stability boundary of the $CHClF_2$ hydrate formed in aqueous $NiCl_2$ solution is located at higher pressure and lower temperature conditions than that of the pure $CHClF_2$ hydrate. This means that the $NiCl_2$ has an inhibition effect on the thermodynamic stability of $CHClF_2$ clathrate hydrates. In addition, I observed that as the concentration of $NiCl_2$ brine soluitions increases, the equilibrium curves of the $CHClF_2$ hydrate in the presence of $NiCl_2$ are shifted into lower temperature and high pressure conditions.

Table 2 Dissociation pressures of $CHClF_2$ hydrates in the presence of $NiCl_2$

$NiCl_2$ (wt%)	T (K)	P (bar)
0	290.1	8.21
	288.0	5.98
	284.8	3.95
	281.3	2.45
	278.2	1.59
5	288.5	7.82
	286.9	6.25
	283.2	3.81
	280.0	2.65
	277.1	1.84
10	286.0	6.83
	285.3	6.06
	282.8	4.19
	278.8	2.77
	276.3	2.03
15	283.7	6.33
	282.2	4.83
	278.7	3.35
	275.2	2.22
	270.7	1.20

3.2 XRD Patterns

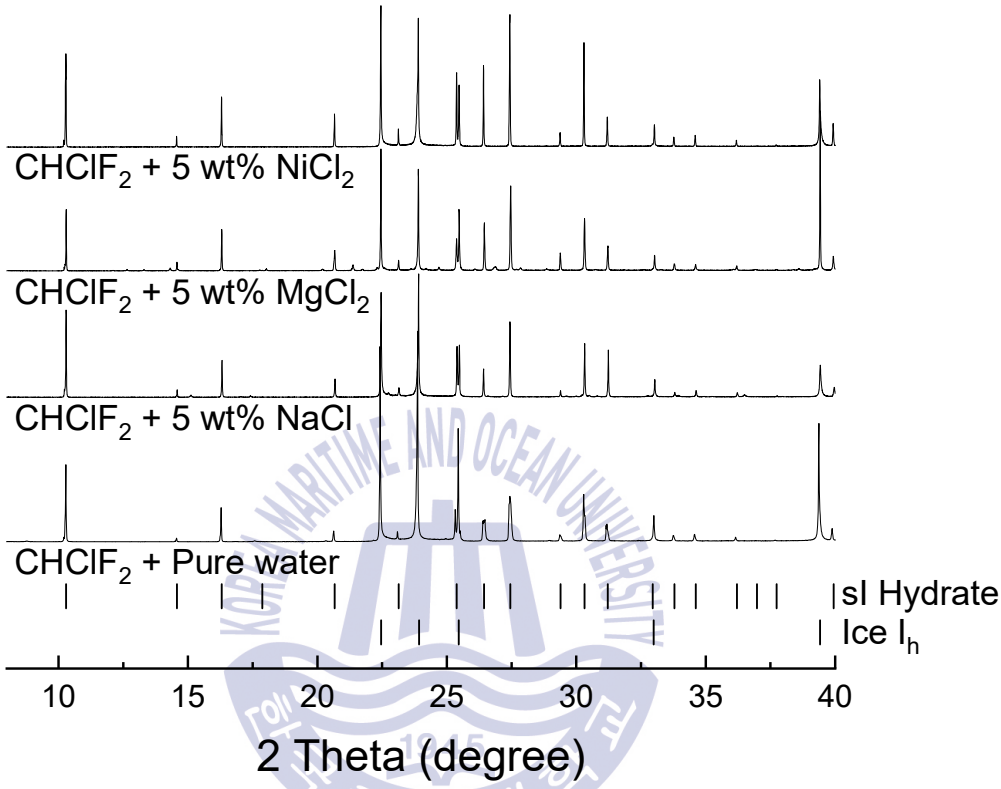

Fig. 14 XRD patterns of $CHClF_2$ hydrates formed in 5 wt% NaCl, $MgCl_2$, and $NiCl_2$, brine solutions and pure water

As shown in Fig. 14, the crystal structures of the $CHClF_2$ hydrates formed in 5wt% NaCl, $MgCl_2$, and $NiCl_2$ brine solutions and pure water were determined from the high-resolution synchrotron XRD. The XRD patterns show that all of the $CHClF_2$ hydrates with and without salt have a structure I clathrate hydrate with a space group *Pm3n*. Lattice parameter and unit cell volume of the $CHClF_2$ hydrates with and without salt are tabulated in Table

3. Based on the XRD results, I confirmed that the $CHClF_2$ hydrates formed in NaCl, $MgCl_2$, and $NiCl_2$ brine solutions had no significant changes in the crystal structure compared with pure $CHClF_2$ hydrates.

Table 3 Crystal Structure, lattice Parameter, and unit cell volume of $CHClF_2$ hydrates under brine environments

$CHClF_2$ hydrate	Structure	Space group	Lattice parameter (Å)	Unit cell volume ($Å^3$)
Pure water	sI	*Pm3n*	*a* =11.990	1723.7
NaCl 5wt%	sI	*Pm3n*	*a* =11.980	1719.4
$MgCl_2$ 5wt%	sI	*Pm3n*	*a* =11.980	1719.4
$NiCl_2$ 5wt%	sI	*Pm3n*	*a* =11.977	1718.1

3.3 Raman Spectra

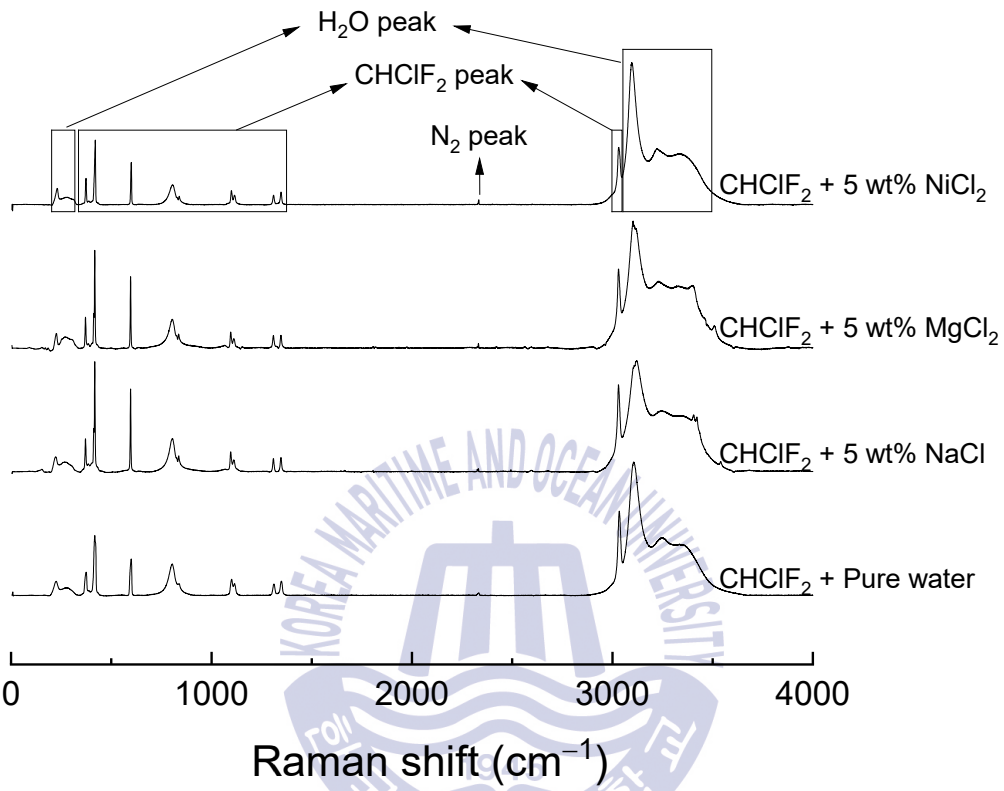

Fig. 15 Raman spectra of $CHClF_2$ hydrates formed in 5 wt% NaCl, $MgCl_2$, and $NiCl_2$, brine solutions and pure water

To explore the structural and intramolecular vibration changes of the $CHClF_2$ hydrates due to the addition of the NaCl, $MgCl_2$, and $NiCl_2$, the Raman spectroscopy measurement was performed. As shown in Fig 15, the Raman bands around 350-1500 cm^{-1} and 3030 cm^{-1} are assigned to the $CHClF_2$ encaged in lage cages of the sI hydrate. In addition, the broad Raman bands around 3000-3500 cm^{-1} represent the O-H vibration of water molecules of the clathrate framework and the spectral range of 200-350 cm^{-1}

is a result of lattice phonon bands of water molecules. Additionally, the small Raman peak at around 2330 cm^{-1} is N－N stretching vibration of N_2 molecules (Murphy & Roberts, 1995) used to make a low temperature environment. Raman spectra of the $CHClF_2$ hydrates formed in 5 wt% NaCl, $MgCl_2$, and $NiCl_2$ brine solutions, when compared with Raman spectra of $CHClF_2$ hydrates formed in pure water, there were no changes in Raman spectra. From the results, I confirmed that the NaCl, $MgCl_2$, and $NiCl_2$ do not effect on the guest ($CHClF_2$) occupation in the hydrate cages and the crystalline structure of $CHClF_2$ hydrates.

The $CHClF_2$ is an asymmetric top molecule which belongs to the point group C_s (Snels & D'Amico, 2001) and intramolecular vibration of $CHClF_2$ is categorized into nine vibration modes (v_1-v_9) (Lefebvre & Anderson, 1992; Merke, et al., 1995). In this study, as shown in Fig 16, noticeable difference in the Raman spectra between solid $CHClF_2$ and $CHClF_2$ clathrate hydrates at the same temperature and pressure were observed in the v_1 and v_4 regions around 3000-3050 cm^{-1} and 750-850 cm^{-1}, respectively, which are assigned to C-H and C-Cl stretching vibrations of $CHClF_2$ molecules trapped in the clathrate cages. Particularly, I explored that the Raman bands in the v_1 region for $CHClF_2$ clathrate hydrates appear at ~16 cm^{-1} lower frequency region than that of the solid $CHClF_2$. It means that the Raman spectra in the v_1 and v_4 regions are the most convincing indication of the clathrate hydrate formation by $CHClF_2$ guests. The v_4 and v_1 vibration mode of the $CHClF_2$ molecules in solid, and hydrates are summarized in Table 4.

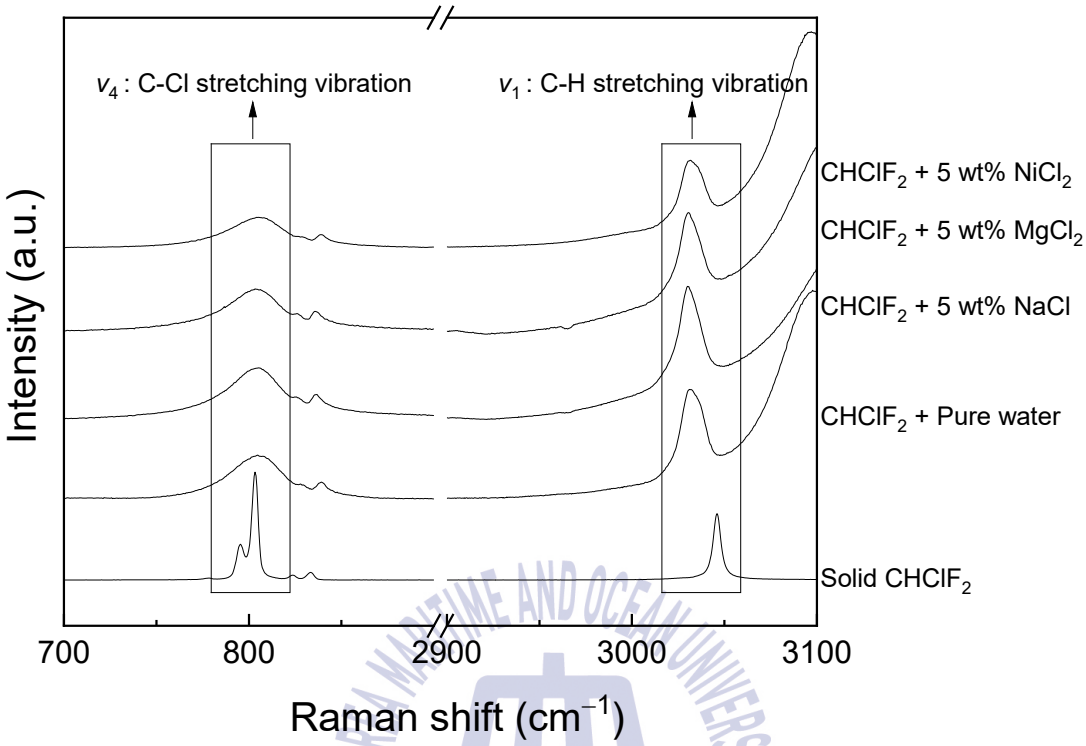

Fig. 16 Enlargement of Raman spectra in the v_4 and v_1 region of $CHClF_2$ encaged in $CHClF_2$ hydrates and solid $CHClF_2$

Table 4 v_4 and v_1 vibration mode of $CHClF_2$ molecules in solid, and hydrates

Assignment	Wavenumber(cm^{-1})				
	Solid (83 K)	$CHClF_2$ hydrate (83 K)	$CHClF_2$ hydrate-NaCl (83 K)	$CHClF_2$ hydrate-$MgCl_2$ (83 K)	$CHClF_2$ hydrate-$NiCl_2$ (83 K)
v_4 (+2 v_6)	796	805	805	805	805
	803	826	826	826	826
	823	837	837	837	837
	833				
v_1	3046	3030	3030	3030	3030

3.4 Hydrate Formation Kinetics

3.4.1 Experimental Results

Fig. 17a, b, c show the experimental results of formation kinetics of the $CHClF_2$ hydrate formed in 0, 5, and 10 wt% NaCl, $MgCl_2$, and $NiCl_2$ brine solutions, respectively. Amount of $CHClF_2$ gas consumed during hydrate formation was calculated from the pressure-volume-temperature (PVT) relationship of the $CHClF_2$. Immediately after the $CHClF_2$ hydrate starts to nucleate, the system pressure rapidly decreases. Slope of the initial P-T data means initial formation rate of the $CHClF_2$ hydrates, and it decreases as the concentration of salts increases, resulting in a reduction in the final pressure at steady state. Thus, it is obvious that the final pressure in hydrate formation is closely related to the three-phase equilibrium pressure. As I have seen in previous chapters, the phase equilibrium condition for $CHClF_2$ hydrate formed from salt solutions was shifted to higher pressure and lower temperature regions as the concentration of the salts in the aqueous solution increases. Therefore, the formation rate of $CHClF_2$ hydrates absolutely depends on the concentration of solution because it shifts the equilibrium boundary, accompanied by changes in the sub-cooling temperature. As I expected, the production rate of $CHClF_2$ hydrates formed from pure water decreases with increasing salinity, which is obviously due to the inhibition effect of the salts on hydrate formation. In addition, the equilibrium pressure of the $CHClF_2$ hydrates formed from salts solutions is shifted to higher pressure conditions, and thus the amount of $CHClF_2$ consumed by hydrate formation also becomes smaller in the presence of salts. This means a reduction in the total amount of pure water produced by hydrate formation in the presence of salts.

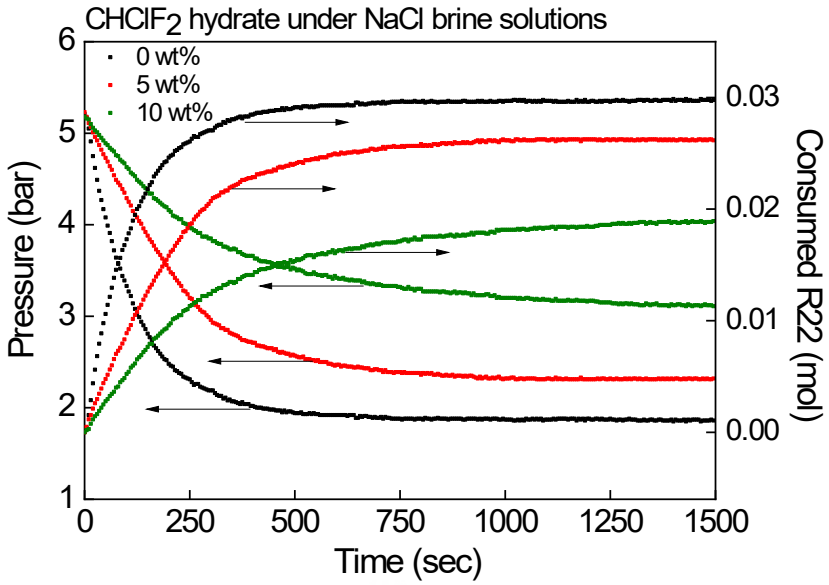

Fig. 17a Formation kinetics of $CHClF_2$ hydrate formed in NaCl brine solutions

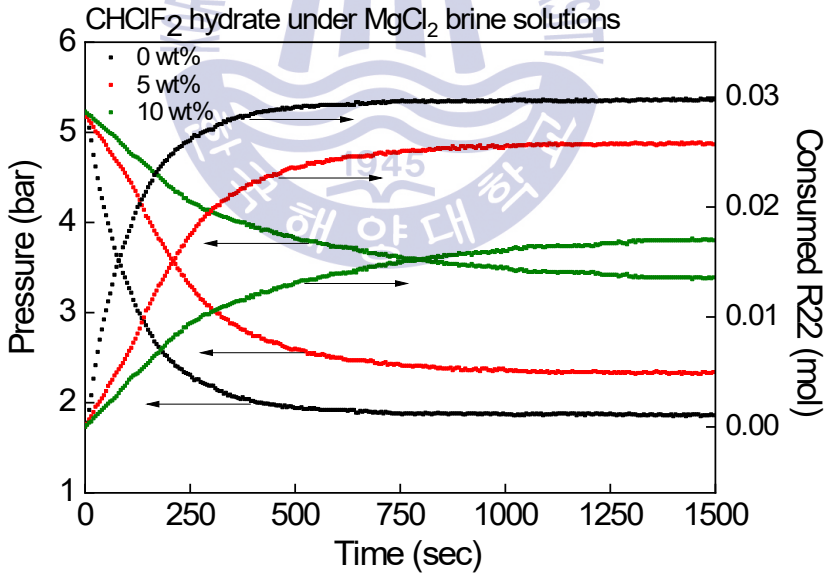

Fig. 17b Formation kinetics of $CHClF_2$ hydrate formed in $MgCl_2$ brine solutions

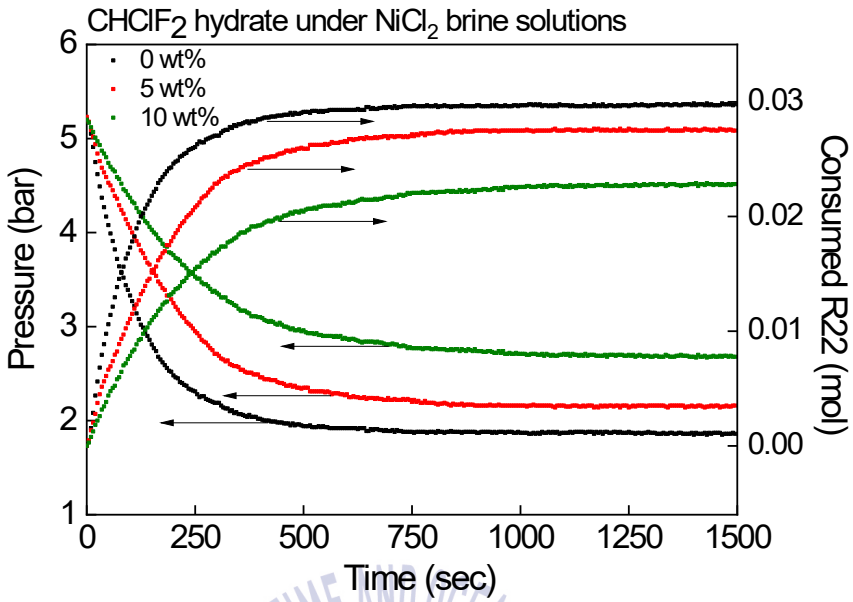

Fig. 17c Formation kinetics of $CHClF_2$ hydrate formed in $NiCl_2$ brine solutions

3.4.2 Kinetic model

In this study, a new kinetic model for theoretically predicting the formation kinetics of $CHClF_2$ hydrates was suggested. When the $CHClF_2$ molecules are encaged in the cavities of the clathrate hydrates, the system pressure P is considered to be directly proportional to the amount of consumed $CHClF_2$ moles. Therefore, it can be expressed as follows:

$$-\frac{dP}{dt} = k'(P - P_{eq}) \quad (1)$$

where P_{eq} is the final equilibrium pressure at the end of the kinetic runs, and k' is the first-order reaction rate constant. The following equation can be derived by integration of the above equation with t:

$$-\ln\left(\frac{P - P_{eq}}{P_0 - P_{eq}}\right) = k't \quad (2)$$

Hydrate growth is affected by three major correlations: intrinsic growth kinetics, mass transfer limitation, and heat transfer limitation (Sloan, 1988). In my experimental systems, diffusion resistance is nearly eliminated by a high agitation speed, and thus the rate controlling achieved an intrinsic reaction (ZareNezhad & Montazeri, 2014). As shown in Fig. 18, the rate constant k' using the Eq. (2) was calculated from the slope of the initial straight line. When using the values of k' and Eq. (2), the calculated time-dependent pressure profile was in a good agreement with the experimental results as shown in Fig. 19a, b, c. According to kinetic model for hydrate particle growth proposed by Englezos et al. (1987), the rate of reaction $r(t)$ can be given as follows:

$$r(t) = \frac{dn}{dt} = k_{app}(f - f_{eq}) \quad (3)$$

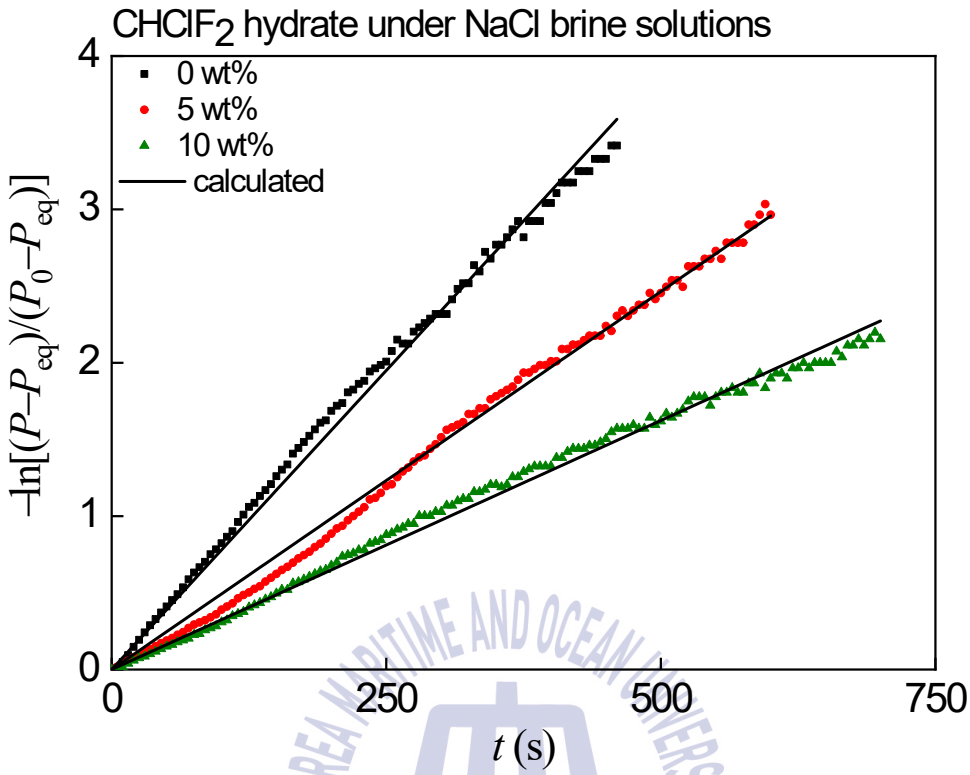

Fig. 18 Plot of the fitting results of experimental data in the initial formation reaction of $CHClF_2$ hydrate formed in NaCl brine solutions

where n is the moles of $CHClF_2$ consumed during the hydrate formation, f is the fugacity of $CHClF_2$ in the gas phase, f_{eq} is the equilibrium fugacity of $CHClF_2$, and k_{app} is the apparent rate constant of the hydrate formation. To consider the contribution to a real gas, the fugacity is expressed by the dimensionless fugacity coefficient as follows:

$$f = P\varnothing \tag{4}$$

In this kinetic model, a Soave-Redlich-Kwong equation of state which has a high accuracy for thermodynamic modeling in the $CHClF_2$ hydrate system was used for calculating the fugacity coefficient (Karamoddin & Varaminian, 2013).

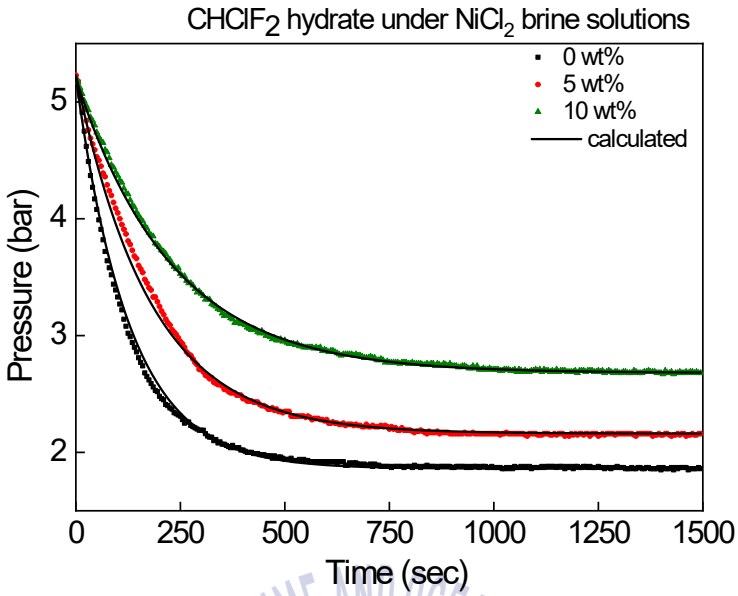

Fig. 19a Formation kinetics of $CHClF_2$ hydrate formed in NaCl brine solutions. Solid lines are the calculated results

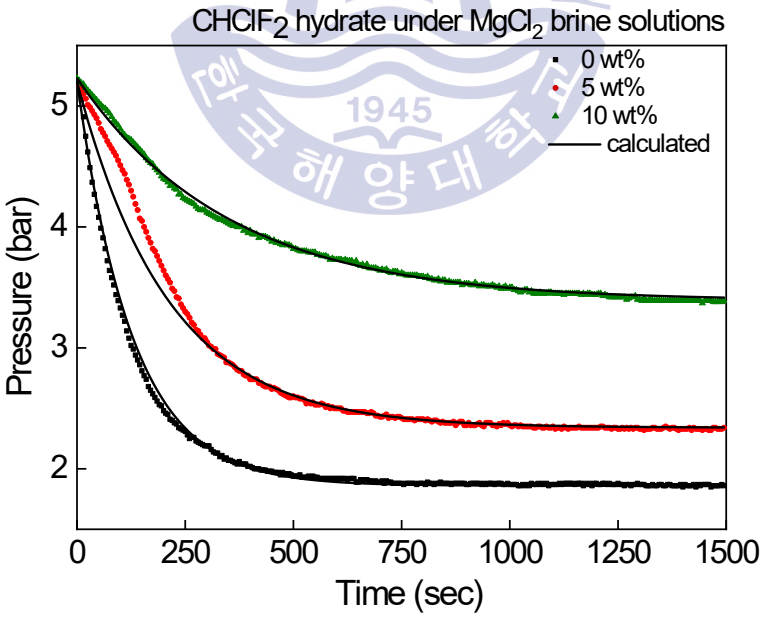

Fig. 19b Formation kinetics of $CHClF_2$ hydrate formed in $MgCl_2$ brine solutions. Solid lines are the calculated results

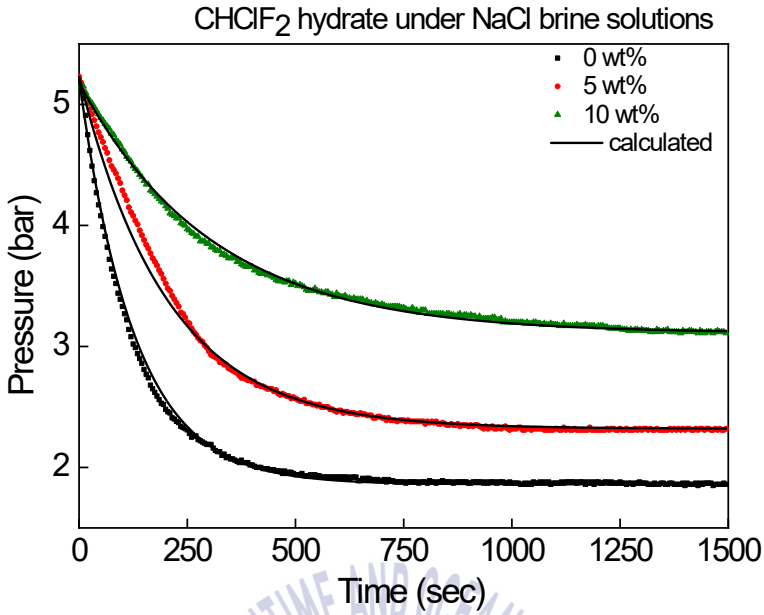

Fig. 19c Formation kinetics of $CHClF_2$ hydrate formed in $NiCl_2$ brine solutions. Solid lines are the calculated results

$$P = \frac{RT}{v-b} - \frac{a(T)}{v(v+b)} \tag{5}$$

The fugacity coefficients of water and $CHClF_2$ can be obtained using Eq. (5) (Soave, 1972).

$$\ln \varnothing = \ln \frac{RT}{P(v-b)} - \frac{a}{bRT} ln\left(\frac{v+b}{v}\right) + Z - 1 \tag{6}$$

The formation kinetics of the clathrate hydrates during the initial period has been used to obtain the apparent rate constant (Englezos, et al., 1987; Hashemi, et al., 2015; Zhang, et al., 2007; Mohammadi, et al., 2014). However, there are many uncertainties at the beginning time of hydrate growth, such as heterogeneous crystal growth, abrupt temperature and pressure variation, and stochastic induction time. To overcome these problems, I proposed a new approach using the transient time-dependent apparent rate constant of hydrate formation. Assuming that the apparent rate constant is nearly constant during the hydrate growth, following equation can be easily obtained by integrating Eq. (3).

$$k_{app} = \frac{n(t)}{\int_0^t [P(t)\varnothing(t) - P_{eq}\varnothing_{eq}]\,dt} \tag{7}$$

Using *n(t)* from the experimental data, *P(t)* from Eq. (2) and $\varnothing(t)$ from Eq. (6), the apparent rate constant k_{app} can be calculated as a function of time.

The apparent rate constant k_{app} during the hydrate formation at the NaCl brine solutions are shown in Fig. 20. The apparent rate constant rapidly increases in the initial period of hydrate growth, up to ~50 s, in all the concentration systems, results of the $NiCl_2$ and $MgCl_2$ system were also same with that. This results can be considered to the dramatic increase of the number of hydrate particles (Zhang et al., 2007). After the initial period, the apparent rate constants are gradually stabilized after ~400 s.

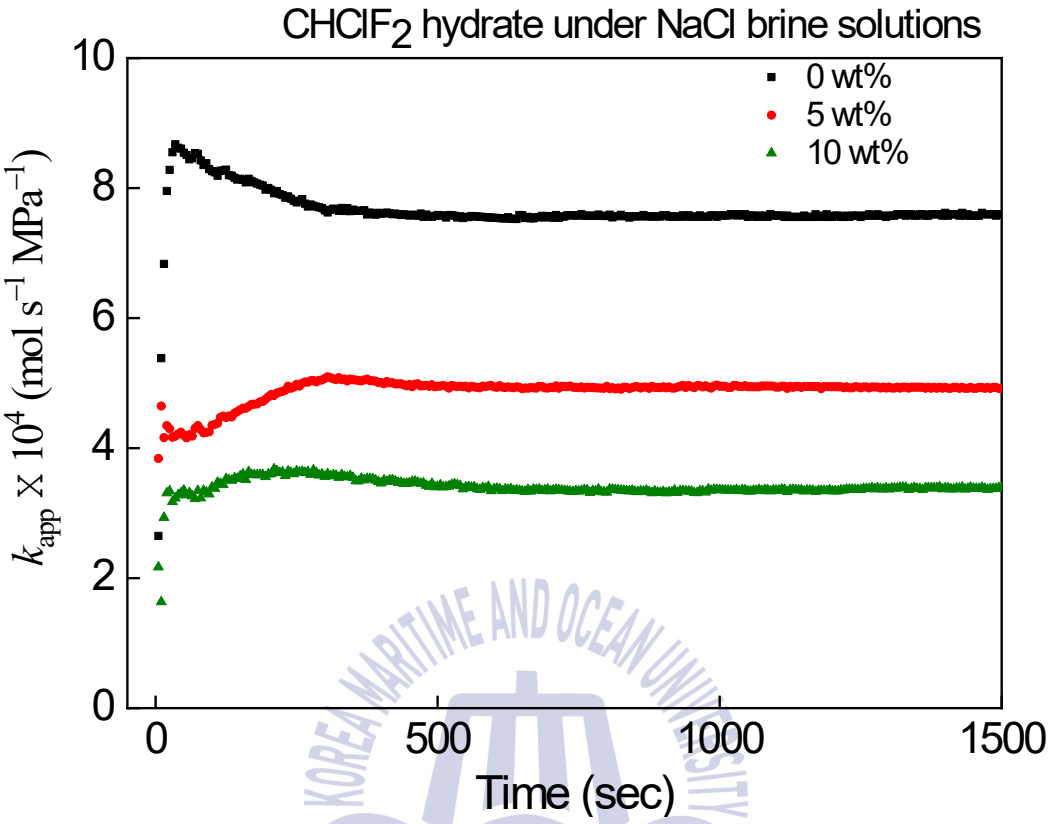

Fig. 20 Apparent rate constant as a function of time during formation of formed in NaCl brine solutions.

The unstable apparent rate constants from 50 to 400 s may be due to the instability of temperature by hydrate formation. It's because, the exothermic reaction of the gas hydrate formation is faster than the heat transfer through the cell. Fig. 21 shows changes in the temperature during the formation reaction of pure R22 hydrate. The cell temperature rapidly increases in the initial stage to a maximum at ~100 s and then gradually decreases with increasing time to the initial cell temperature. This is definitely caused by the exothermic nature of the gas hydrate formation reaction, leading to possible errors in calculating the apparent rate constant at the beginning time.

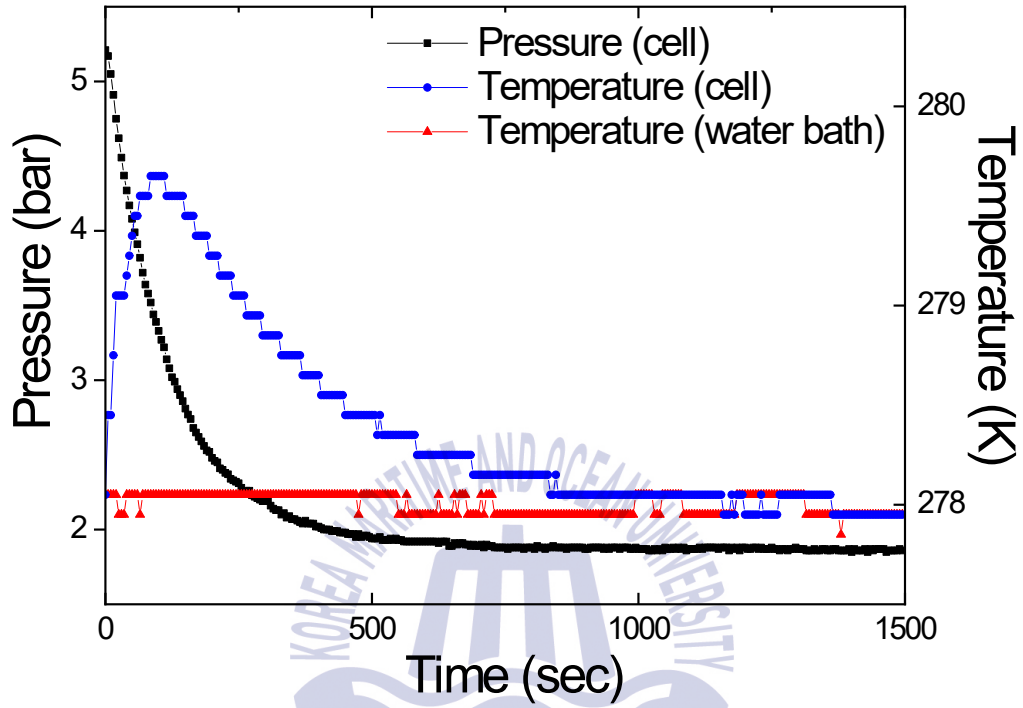

Fig. 21 Change in temperature and pressure during R22 hydrate formation at an initial pressure and temperature of 5.21 bar and 278 K

The apparent rate constants were finally stabilized with a steady state value after ~1,500 s and using this apparent rate constant at the steady state, I calculated the mole numbers of consumed $CHClF_2$ during hydrate formation and compared with the experimental data. As shown in Fig 22a, b, c, the predicted results are in a good agreement with the experimental kinetics, even though there is a slight deviation at the initial stage. The kinetic parameters for the formation of the $CHClF_2$ hydrate formed in NaCl, $MgCl_2$, and $NiCl_2$ brine solutions are tabulated in Table 5. Fig. 23 shows the apparent rate constants as a function of salt concentration for $CHClF_2$ hydrates, indicating that they linearly decrease with an increase of the salinity of solutions. It means that the apparent rate constants are significantly affected by salt concentration during the formation of $CHClF_2$ hydrates.

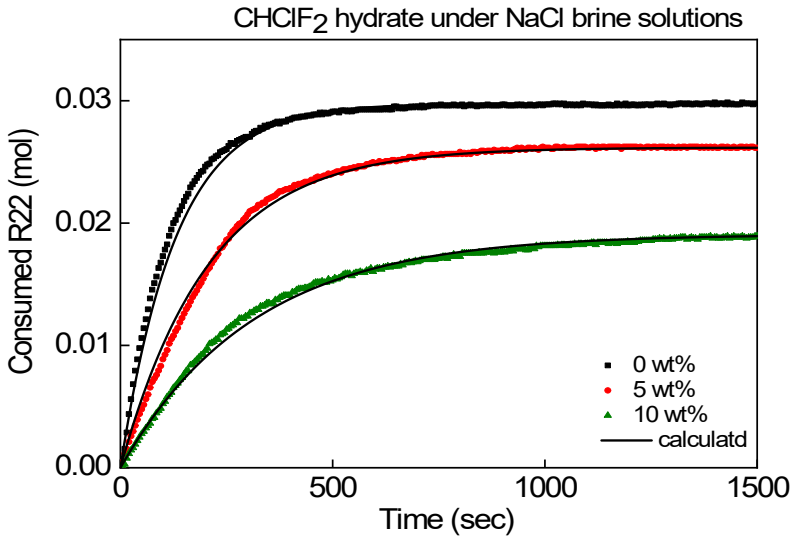

Fig. 22a Comparison of experimental and calculated formation kinetics of $CHClF_2$ hydrates formed in NaCl brine solutions.

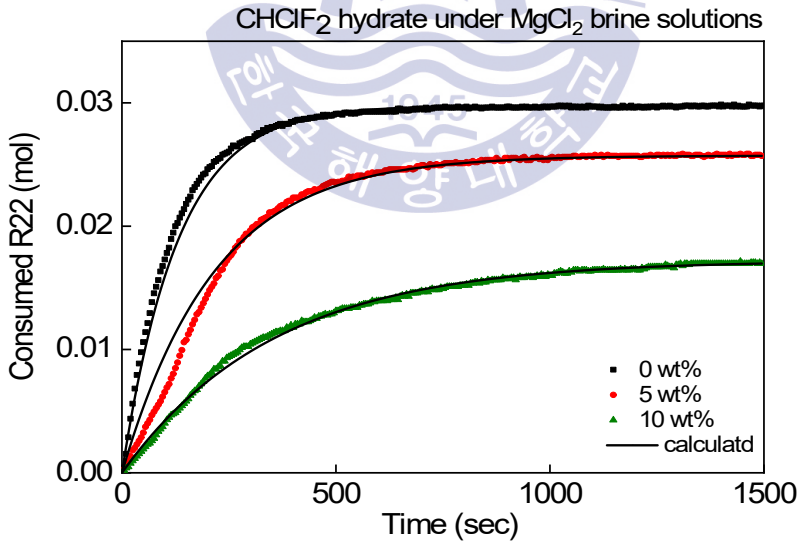

Fig. 22b Comparison of experimental and calculated formation kinetics of $CHClF_2$ hydrates formed in $MgCl_2$ brine solutions.

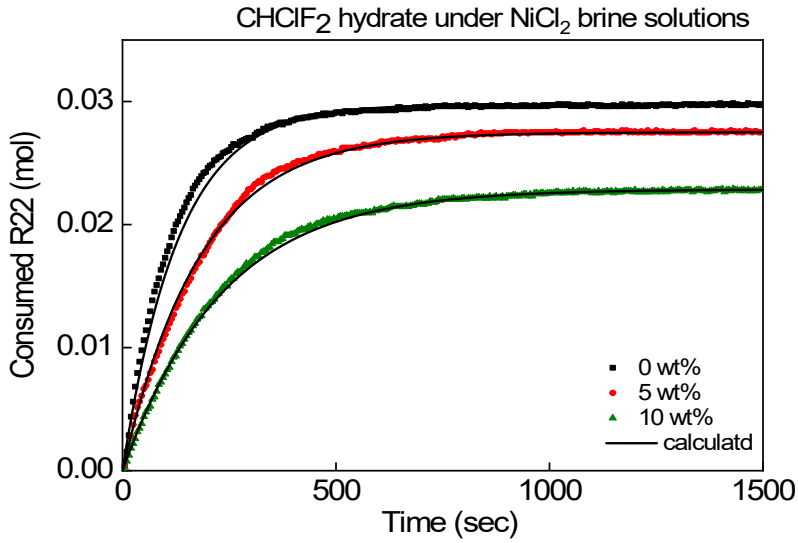

Fig. 22c Comparison of experimental and calculated formation kinetics of $CHClF_2$ hydrates formed in $NiCl_2$ brine solutions.

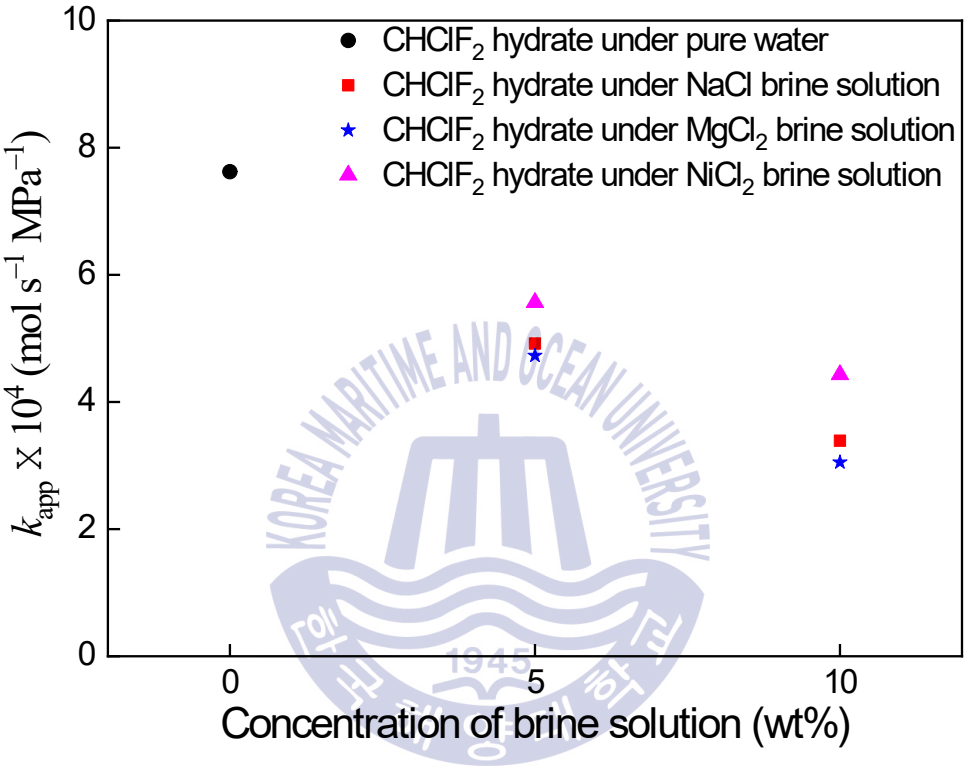

Fig. 23 Relationship between concentration of the brine solution and apparent rate constant from formation kinetics at 278 K

Table 5 Kinetic parameters for formation of $CHClF_2$ hydrates in the presence of NaCl, $MgCl_2$, and $NiCl_2$, respectively

Hydrate system	T (K)	P_0 (MPa)	P_{eq} (MPa)	$k' \times 10^3 (s^{-1})$	$r^{ini} \times 10^4$ (mol s^{-1})	$k_{app} \times 10^4$ (mol $s^{-1}MPa^{-1}$)
Pure $CHClF_2$	278	0.521	0.186	7.80	2.19	7.60
$CHClF_2$ + 5 wt % NaCl	278	0.523	0.232	4.93	0.98	4.92
$CHClF_2$ + 10 wt % NaCl	278	0.518	0.311	3.25	0.55	3.39
$CHClF_2$ + 5 wt % $MgCl_2$	278	0.520	0.234	4.74	0.66	4.73
$CHClF_2$ + 10 wt % $MgCl_2$	278	0.523	0.339	2.86	0.39	3.05
$CHClF_2$ + 10 wt % $NiCl_2$	278	0.520	0.216	5.60	1.98	5.54
$CHClF_2$ + 10 wt % $NiCl_2$	278	0.520	0.268	4.02	1.04	4.11

Chapter 4. Conclusion

In summary, I investigated the three phase (hydrate-aqueous liquid-vapor) equilibria of the $CHClF_2$ hydrate formed in $NiCl_2$ brine solutions. The result shows that upon increasing the $NiCl_2$ concentration, the hydrate stability boundary was shifted to lower pressure and higher temperature conditions. It indicate the inhibition effect of the $NiCl_2$ on the thermodynamic stability of the $CHClF_2$ clathrate hydrate.

I also observed the crystal structure and guest occupation behaviors of the $CHClF_2$ molecules in the $CHClF_2$ hydrate formed in NaCl, $MgCl_2$, and $NiCl_2$ brine solutions using the XRD and Raman spectroscopy measurement. There are no changes compared with pure $CHClF_2$ hydrate; therefore, I concluded that the NaCl, $MgCl_2$, and $NiCl_2$ has no significant effect on the $CHClF_2$ hydrate structures and guest occupation behaviors in the clathrate cages. It means that the NaCl, $MgCl_2$, and $NiCl_2$ do not participate in the $CHClF_2$ hydrate framework; thus, the hydrate-based method using $CHClF_2$ guest can be used to seawater desalination and removing $NiCl_2$ from the electroplating effluents.

Finally, I confirmed that the new kinetic model for theoretically predicting the formation kinetics of $CHClF_2$ hydrates can describe the experimental results very well. These experimental results and interpretations provide fundamental information into the HBD processes.

감사의 글

이 논문을 마지막으로 길고도 짧았던 석사과정의 끝이 다가왔다는 것이 실감이 나질 않습니다. 다만, 아무것도 모르던 제가 이 과정을 무사히 마칠 수 있었던 것은 주변의 많은 도움과 격려가 있었기 때문이라는 것은 분명히 알 수 있을 것 같습니다.

석사 과정동안 학문적인 부분은 물론이고 인생에 대한 훌륭한 가르침을 주셨던 윤지호 교수님께 깊은 감사의 말씀을 전합니다. 교수님의 지도 덕분에 석사생으로서 경험할 수 있는 다양하고 멋진 일들을 경험할 수 있었고 이러한 경험들은 제 인생에 있어 큰 밑거름이 되리라 믿어 의심치 않습니다. 학문에 대한 열정이 넘치시는 교수님을 지켜보며 연구자의 길이 무엇인지 어렴풋이 알게 되었으며, 어떤 일을 하던지도 그 열정을 본받고 싶습니다. 진심으로 존경하고 감사드립니다.

공동 지도교수님으로서 끊임없이 격려해주셨던 한국해양과학기술원의 김동선 교수님께 감사드립니다. 또한 제 부족한 논문을 심사해주시고 피드백 해주신 유경근 교수님께도 진심으로 감사의 말씀을 전합니다. 매학기 대학원 세미나를 통해 저를 더욱 성장 할 수 있도록 도와주셨던 장원일 교수님, 신성렬 교수님, 임종세 교수님, 그리고 정우근 교수님께도 감사의 말씀을 전하고 싶습니다. 학부과정 때 교수님들께서 알려주셨던 것들이 하나도 빠짐없이 모두 제 석사과정의 연구에 피와 살이 되었다 생각됩니다.

실험실에 관한 모든 것들을 잘 알려줬던 동훈이 오빠, 이제 실험실에 없어서는 안 될 재학이, 실험실 막내 똑똑이 지영이, 어려움이 있을 때 항상 도와주셨던 병수선배, 실험실 선배이자 항상 많은 도움을 주셨던 숙현이 언니에게 감사드립니다. 그리고 혼자서 힘이 들 때 츤데레처럼 챙겨줬던 대철이 오빠, 함께 고민을 나눈 경남이 언니, 항상 긍정적인 응원을 해준 현지, 대학원생활에 많은 도움을 줬던 준석이 오빠와 윤주, 멀리 있지만 힘이 되어준 창키에게도 진심으로 감사하다는 말 전합니다.

또한, 혼자일 뻔한 일본에서 좋은 추억을 함께 나눈 효진이 언니, 서윤이, 한때 기숙사 멤버였던 영일이 오빠, 밤늦게 차를 태워다줬던 다운이 오빠, 바쁜 와중에 실험

장치에 대해 많이 알려줬던 주미, 수진이, 그리고 수윤이 오빠, 영준이 오빠, 이번에 신입생이 될 국호, 현진이, 서영이, 특히 물탐에 가면 항상 반겨주는 경민이, 마지막으로 대학생활의 활력소가 되어준 예리, 이 글에 모든 분들의 이름을 다 담진 못했지만 함께 해주셨던 모든 분들께 진심으로 감사의 말씀을 드립니다. 덕분에 힘들었던 대학원생활을 행복하게 보낼 수 있었던 것 같습니다.

마지막으로 저를 항상 사랑해주시고 제 편이 되주는 우리 가족, 아빠, 엄마, 재하오빠에게 진심으로 감사드립니다. 앞으로도 믿고 응원해주시길 바라며 부끄럽지 않은 딸, 동생이 되도록 노력하겠습니다. 사랑하고 감사합니다.

Reference

Ahn, K.H., Song, K.G., Cha, H.Y. & Yeom, I.T., 1999. Removal of ions in nickel electroplating rinse water using low-pressure nanofiltration. *Desalination*, 122, pp.77-84.

Al-Wazzan, Y. & Al-Modaf, F., 2001. Seawater desalination in Kuwait using multistage flash evaporation technology–historical overview. *Desalination*, 134, pp.257-267.

Andrea, C., Giorgio, M. & Lucio, R., 2009. *Seawater Desalination: Conventional and renewable energy processes*. Springer Science & Business Media.

Atwood, J.L., Davies, J.E.D. & MacNicol, D.D., 1984. *Inclusion Compound*. Academic Press: London.

Babu, P. et al., 2018. A Review of Clathrate Hydrate Based Desalination To Strengthen Energy－Water Nexus. *ACS Sustainable Chem. Eng.*, 6, pp.8093-8107.

Berecz, E. & Bella-Achs, M., 1983. *Gas hydrates*. Elsevier, Amsterdam.

Benvenuti, T. et al., 2014. Recovery of nickel and water from nickel electroplating wastewater by electrodialysis. *Sep. Purif. Technol.*, 129, pp.106-112.

Chun, M.K. & Lee, H., 1998. Phase equilibria of R22 ($CHClF_2$) hydrate system in the presence of sucrose, glucose and lactic acid. *Fluid Phase Equilibria*, 150, pp.361-370.

Chun, M.K., & Lee, H., 2000. Phase Equilibria of R22 ($CHClF_2$) Hydrate

Systems in the Presence of NaCl, KCl, and $MgCl_2$. *J. Chem. Eng. Data*, 45(6), pp1150-1153.

Darre, N.C. & Toor, G.S., 2018. *Desalination of Water: a Review*. Springer International Publishing AG.

Davidson, D.W. et al., 1986. Laboratory analysis of a naturally occurring gas hydrate from sediment of the Gulf of Mexico. *Geochim. Cosmochim. Acta.*, 50, pp.619-623.

Dong, Z. et al., 2015. Development of lower cost seawater desalination processes using nanofiltration technologies — A review. *Desalination*, 376, pp.109-116.

Englezos, P., Dholabhai, P., Kapgeralos, N. & Bishnoi, P.R., 1987. Kinetics of formation of methane and ethane gas hydrates. *Chem. Eng. Sci.*, 42, pp.2647-2658.

Eslamimanesh, A., Mohammadia, A.H. & Richon, D., 2011. Thermodynamic model for predicting phase equilibria of simple clathrate hydrates of refrigerants. *Chem. Eng. Sci.*, 66, pp.5439-5445.

Eveloy, V., Rodgers, P. & Qui, L., 2015. Hybrid gas turbine–organic Rankine cycle for seawater desalination by reverse osmosis in a hydrocarbon production facility. *Energy Convers. Manag.*, 106, pp.1134-1148.

Ganji, H. et al., 2007. Effect of different surfactants on methane hydrate formation rate, stability and storage capacity. *Fuel,* 86, pp.434-441.

Hamed, O.A., 2005. Overview of hybrid desalination systems–Current status and future prospects. *Desalination*, 186, pp.207-214.

Hammerschmidt, E.G., 1934. Formation of gas hydrates in natural gas Transmission lines. *Ind. Eng. Chem.*, 26, pp.851-855.

Hashemi, H. et al., 2015. Experimental study and modeling of the kinetics of refrigerant hydrate formation. *J. Chem. Thermodyn.*, 82, pp.47-52.

Javanmardi, J., Nasrifar, Kh., Najibi, S.H. & Moshfeghian, M., 2005. Economic evaluation of natural gas hydrate as an alternative for natural gas transportation. *Appl. Therm. Eng.*, 25, pp.1708-1723.

Jeffrey, G.A., 1984. Hydrate inclusion compound. *J. Incl. Phenom.*, 1, pp.211-222.

Kalogirou, S.A., 2005. Seawater desalination using renewable energy sources. *Prog. Energy Combust. Sci.*, 31, pp.242-281.

Karamoddin, M. & Varaminian, F., 2013. Experimental measurement of phase equilibrium for gas hydrates of refrigerants, and thermodynamic modeling by SRK, VPT and CPA EOSs. *J. Chem. Thermodynamics*, 65, pp.213-219.

Karamoddin, M., Varaminian, F. & Daraee, M., 2014. Kinetic study on the process of $CHClF_2$ (R22) hydrate formation in the presence of SDS surfactant based on chemical affinity. *J. Nat. Gas Sci. Eng.*, 9, pp.46-51.

Lefebvre, J.H. & Anderson, A., 1992. Raman study of a phase transition in solid chlorodifluoromethane. *J. Raman. Spectrosc.*, 23, pp.243-247.

Murphy, P.J. & Roberts, S., 1995. Laser Raman Spectroscopy of Differential Partitioning in Mixed-Gas Clathrates in $H_2O-CO_2-N_2-CH_4$ Fluid

Inclusions: Implications for Microthermometry. *Geochim. Cosmochim. Acta*, 59, pp.4809-4824.

Merke, I. et al., 1995. High-resolution FT-IR spectra of CHF_2Cl in the region between 335 and 450 cm^{-1}. *J. Mol. Spectrosc.*, 173, pp.463-476.

Mezher, T., Fath, H., Abbas, Z. & Khaled, A., 2011. Techno-economic assessment and environmental impacts of desalination technologies. *Desalination*, 266. pp.263-273.

Mohammadi, A. et al., 2014. Kinetic study of carbon dioxide hydrate formation in presence of silver nanoparticles and SDS. *Chem. Eng. J.*, 237, pp.387-395.

Oki, T. & Kanae, S., 2006. Global hydrological cycles and world water resources. *Science*, 313, pp.1068-1072.

Park, K. et al., 2011. A new apparatus for seawater desalination by gas hydrate process and removal characteristics of dissolved minerals (Na^+, Mg^{2+}, Ca^{2+}, K^+, B^{3+}). *Desalination*, 274, pp.91-96.

Ripmeester, J.A., Tse, J.S., Ratcliffe, C.I. & Powell, B.M., 1987. A new clathrate hydrate structure. *Nature*, 325, pp.135-136.

Sloan, E.D., 1988. *Clathrate hydrates of natural gases*. 3th ed. Marcel Dekker, New York.

Sloan, E.D., 2003. Fundamental Principles and Applications of Natural Gas Hydrates. *Nature*, 426, pp.353-363.

Snels, M. & D'Amico, G., 2001. Diode laser jet spectra and analysis of the ν_3 and ν_8 fundamentals of CHF_2Cl. *J. Mol. Spectrosc.*, 209, pp.1-10.

Soave, G., 1972. Equilibrium constants from a modified Redlich-Kwong equation of state. *Chem. Eng. Sci.*, 27, pp.1197-1203.

Seo, Y. et al., 2015. Equilibrium, kinetics, and spectroscopic studies of SF_6 hydrate in NaCl electrolyte solution. *Environ. Sci. Technol.*, 49, pp.6045-6050.

Song, Y. et al., 2016. Hydrate-based heavy metal separation from aqueous solution. *Scientific Reports*, 6, pp.21389.

Udachin, K.A., Ratcliffe, C.I. & Ripmeester, J.A., 2002. Single Crystal Diffraction Studies of Structure I, II and H Hydrates: Structure, Cage Occupancy and Composition. *J. Supramol. Chem.*, 2, pp.405-408.

UNEP, 2000. *The montreal protocol on substances that deplete the ozone layer*. ISBN 92-807-1888-6.

Van der Bruggen, B. & Vandecasteele, C., 2002. Distillation vs. membrane filtration: overview of process evolutions in seawater desalination. *Desalination*, 143, pp.207-218.

VirgiliPankratz, F. & Gasson, T.J., 2016. *IDA desalination yearbook 2015-2016*. Oxford, UK: Global Water Intel.

von Stackelberg, M., 1949. Feste Gas hydrate, *Naturwissenschaften*, 36(11), pp.327-333.

Wittstruck, T.A., Brey, W.S., Buswell, A.M. & Rodebush, W.H., 1961. Solid hydrates of some halomethanes. *J. Chem. Eng. Data*, 6, pp.343-346.

Yu, N.-T. & Krimm, S., 1977. Raman Spectroscopy: A Conformational Probe in Biochemistr. *Crit. Rev. Biochem. Mol. Biol.*, 4(3), pp.229-280.

ZareNezhad, B. & Montazeri, V., 2014. Development of a high efficient gas to hydrate (GTH) conversion process using SDS kinetic promoter for maximizing the CO_2 recovery with minimum energy consumption. *Energy Conv. Manag.*, 79, pp.289-293.

Zhang, J.S., Lee, S. & Lee, J.W., 2007. Kinetics of methane hydrate formation from SDS solution. *Ind. Eng. Chem. Res.*, 46, pp.6353-6359.

Zhong, Y. & Rogers, R.E., 2000. Surfactant effects on gas hydrate formation. *Chem. Eng. Sci.*, 55, pp.4175-4187.